Components of Variance in Brain Perfusion and the Design of Studies of Individual Differences: The Baseline Study

Roberto Viviani,* Eun-Jin Sim,* Hanna Lo,* Sven Richter,*

Sebastian Haffer,* Nadine Osterfeld,* Jan Thöne,[+] Georg Grön,*

Petra Beschoner*

* Department of Psychiatry III
University of Ulm
[+] Universitätsklinik für Neurologie,
St. Josef Hospital, Klinik der Ruhr-Universität Bochum

Corresponding author:
Dr Roberto Viviani, PhD
Department of Psychiatry III
University of Ulm
Leimgrubenweg 12
89075 Ulm, Germany
Telephone: +49 731 50061569
E-mail: roberto.viviani@uni-ulm.de

Components of Variance in Brain Perfusion and the Design of Studies of Individual Differences: The Baseline Study

Abstract

Simple baseline studies correlate average perfusion levels measured at rest with individual variables, or contrast subject groups as in case-control studies. In this methodological work, we summarize some formal properties of the design of these studies, and investigate the sources of variance that characterize data acquired with the arterial spin labelling technique, with the purpose of alerting users to the main sources of variation that determine background variance and affect the power of statistical tests. This design typology is characterized by two variance components: between acquisitions and between subjects. We show that variation between acquisitions is affected by the presence of large vessels and venous sinuses, with potential adverse effects especially in the temporal and insular regions, and provide maps of the number of acquisitions or subjects required to reach the desired estimate precision. Furthermore, we show that the largest source of variation between subjects is captured by global perfusion levels, and can in principle be removed by adjusting the data. Significance levels, however, are not always only improved by the adjustment procedure; we provide an example in the correlation with age, and attempt to explain the consequences of the adjustment with the help of a principal component analysis of the data. We also show the existence of variation between subjects in the perfusion in the territory of the posterior cerebral artery and in hemispheric asymmetry.

Components of Variance in Brain Perfusion and the Design of Studies of Individual Differences: The Baseline Study

Introduction

Arterial spin labeling (ASL) is a magnetic resonance imaging technique for the estimation of regional blood perfusion (rCBF) in the brain (see Buxton 2002 for a comprehensive introduction). This technique is particularly appropriate in the study of states or conditions lasting one minute or longer (Aguirre et al. 2002). Unlike positron emission tomography (PET), ASL allows the convenient and economical acquisition of quantitative brain imaging data without exposing participants to ionizing radiation. Furthermore, the spatial and temporal definition of ASL is generally superior to that of PET. However, until recently, technical limitations prevented the acquisition of more than a small number of slices. These limitations have been superseded by the introduction of new ASL sequences that maintain the dose of transferred energy within acceptable limits (such as the continuous arterial spin labeling sequence, CASL, introduced by Wang et al. 2005).

This study concerns the application of the CASL technique in the baseline condition. In this condition, participants are placed in the scanner and are asked to lie quietly and rest without falling asleep. Studies of baseline brain activity have a history going back to PET studies of baseline metabolism, both in normal subjects, where the effect of individual variables such as gender or age was investigated (see Tumeh et al. 2007, Willis et al. 2002 for recent reviews), and in neurological and psychiatric disorders such as depression, to name one example (Drevets 2000, Mayberg 2003). More recently, baseline cerebral metabolism has also been shown to involve relative activation of medial and temporoparietal cortical areas

(Shulman et al. 1997), thought to reflect the operation of a 'default mode network' during rest (Raichle et al. 2001). Because of their safety and practicality, the CASL technique is a promising methodology for the study of the issues raised by the baseline condition (see for example Abler et al. 2008; Beschoner et al. 2008; O'Gorman et al. 2006; Rao et al. 2007).

An important issue in the design of any study is the way in which variance in the data arising from unknown variables or experimental error may be controlled to improve the capacity of the statistical test to detect the effect of interest. Understanding this aspect of study design requires, on the one hand, considering the formal aspects of the model, and on the other, knowledge about the magnitude and spatial distribution of undesired variance in the data. The issues discussed here apply to all designs that are formally identical to the baseline study, i.e. studies of individual variance where only one condition is measured, and there is no within-subjects explanatory or experimental variable. In contrast to most experimental studies, baseline studies focus on between-subjects variables such as belonging to a patient or control group, or any other variable measured on the individuals.

The random effects model corresponding to the simple baseline design contains two sources of variance: acquisition-to-acquisition and subject-to-subject variation. In the following, our objective is the characterization of these variance components in the perfusion images of a sample of 228 healthy young subjects. These two sources of variance may be of interest to experimenters, because they give indication of the gains in the precision of estimates obtained by increasing the duration of acquisition sessions (Snedecor and Cochran 1967). Differences in these quantities in different parts of the brain determine differences in the power of statistical tests, and therefore of the regional sensitivity of the ASL technique. In particular, we will be concerned with showing the impact of the presence of large vessels in the variance of the perfusion signal, demonstrating the existence of a relationship between macroscopic anatomy and signal variance in the images obtained with this technique.

We will further explore the spatial characteristics of subject-to-subject variance through component analyses of the averages images in each subject (the input to the second-level analysis). This analysis will demonstrate the existence of components of variation related to the distribution of vascular territories, and the differential impact of global perfusion levels on white and grey matter. We will then show the relation between these components of variation and individual variables such as age and gender.

A further issue about which we seek clarification is the impact of adjusting for global cerebral perfusion values (gCBF) by adding them as a covariate in the analysis (Friston et al. 1990, Macey et al. 2004). Adjustment for gCBF is a pragmatic attempt to handle variance associated with a random effect of volumes and its interaction with a voxel factor without modeling this effect explicitly, which would involve abandoning the SPM modeling strategy. This procedure is designed to remove global perfusion signal changes that, by increasing the variance of the signal, can reduce the sensitivity of the statistical test (Arndt et al. 1996, Gavrilescu et al. 2002). While the literature on adjusting for gCBF levels is concerned with its impact on the within-subjects effects of experimental manipulations, we will be here specifically concerned with its impact on the inference about between-subjects variables, and will correspondingly attempt to identify the subject-to-subject variation removed by the adjustment. A case study of the association between regional perfusion levels and age will illustrate the effect of adjusting for gCBF levels in terms of its impact on separate components of variance. We will also show that gCBF levels commonly correlate with individual variables, so that the ensuing analyses (with and without adjustment) provide qualitatively different indications about the association between perfusion levels and the individual variable of interest.

Material and methods

Recruitment

Participants were recruited from local schools and university and by local announcements. Exclusion criteria were neurological or medical conditions, use of medication, or a history of mental illness, and subclinical structural abnormalities. The study is based on 228 right-handed participants (101 males) aged between 17 and 52 years at the time of the scan (mean age 24.7, std. dev. 5.4) who gave informed consent. The study protocol was approved by the local ethical committee and was in compliance with national legislation and the Code of Ethical Principles for Medical Research Involving Human Subjects of the World Medical Association.

Data acquisition

All magnetic resonance imaging (MRI) data were obtained with a 3-Tesla Magnetom Allegra (Siemens, Erlangen, Germany) MRI system equipped with a head volume coil. All participants were scanned at the Department of Psychiatry of the University of Ulm. A standard T2-weighted structural brain scan from the clinical screening routine in use in our hospital (TR 4120, TE 82) was taken on all participants to exclude subclinical structural abnormalities. A continuous arterial spin-labeling technique was used as described in Wang et al. (2005). Interleaved images with and without labeling were acquired for 8 min (120 acquisitions) by using a gradient-echo echo-planar imaging sequence with a field of view of 22 cm. Image size was $64 \times 64 \times 15$ voxels, slice thickness 6 mm with a gap of 1.5 mm, giving a voxel size of $3.44 \times 3.44 \times 7.50$ mm. The images were acquired with an echo-planar imaging sequence (EPI) with TR 4000, TE 17, anterior-to-posterior phase encoding, a flip angle of 90°, and a bandwidth of 3005 Hz/Pixel. A delay of 1 sec was inserted between the end of the labeling pulse and image acquisition to reduce transit artifacts. The SPM2 package was used (Wellcome Department of Cognitive Neurology, London; online at http://www.fil.ion.ucl.ac.uk) for realignment and stereotactic normalization to an EPI

template (Montreal Neurological Institute, resampling size: $2 \times 2 \times 2$ mm). Reconstruction of rCBF values was obtained using the Perf_resconstruct_V02 SPM add-on software by H. Y. Rao and J. J. Wang, from the Department of Radiology and Center for Functional Neuroimaging at University of Pennsylvania (online at http://www.cfn.upenn.edu/perfusion/software.htm). The software implements eq. (1) of Wang et al. (2003). The 'simple subtraction' method was used. All volumes were smoothed using an isotropic Gaussian kernel of full width half-maximum (FWHM) of 6 mm prior to the principal component analysis. An explicit mask was obtained by combining an *a priori* thresholded tissue probability maps provided by the SPM package at 0.25 for gray or white matter with another mask thresholding the standard deviation of the mean images to less than 25 (as described in the text). Furthermore, slices lower than $z = -24$ mm. were excluded, since very low slices have very large variance in our data (these slices are close to where the labeling pulse was given). We also excluded slices above $z = 48$ mm. to prevent lack of coverage of the top of the brain in some individuals to influence the outcome of the principal component analysis.

Time-of-flight (TOF) angiography images were obtained from a subset of 42 participants (13 males) aged between 18 and 52 (mean age 28, std. dev. 9). A T1-weighted imaging sequence was used with a TR 41, TE 4.92, flip angle 90, and bandwidth 110 Hertz/Pixel. Image size was $512 \times 640 \times 56$ voxels, slice thickness 1.8 mm with a gap of 18 mm between slices. These parameters correspond to a standard clinical TOF image, with the exception that no saturation band was present in our sequence. This band is usually applied at the upper part of the cerebrum to suppress signal from venous sinuses, which is present in our images. These images were normalized to a template prepared as the mean of the original images.

Statistical analysis

After preprocessing, standard ANOVA estimators in a one-way random effect model were used to compute the acquisition-to-acquisition and subject-to-subject variance components. Principal component analysis was carried out using standard methods, summarized in the Appendix of Viviani et al. (2005). Data were single-centered voxel by voxel, thus considering voxels to be 'variables' and the average individual volumes to be 'observations' in the usual principal component terminology (Jolliffe 1986). The principal component analysis delivers the spatial components ('eigenimages'), and a principal component score, one for each volume. This score is the inner product between the eigenimage and the rCBF values in each voxel of the volume, and represents the extent to which each volume displays the pattern identified by the component. The correlation of gCBF, age, and gender of each average subject image with these the principal component scores therefore provides a summary measure of how the spatial patterns of variation of the components may be related to individual variables.

In the analysis of the perfusion modeled as an effect of age, volumes were averaged in each individual to obtain an estimate of the baseline perfusion, which was entered at the 'second level' of analysis to model subjects as a random factor. Because of the lack of temporal autocorrelation in the signal obtained with the simple subtraction method (Aguirre et al. 2002, Mumford et al. 2006), the individual averaging procedure yields valid tests and correct ANOVA estimates of variance components. When indicated, adjustment for the global signal level was obtained by including a centered covariate in the model containing global perfusion levels estimated as the average perfusion within the masked region. No scaling procedures such as 'grand mean scaling' were applied to the data. Second level statistical analysis was performed on these averaged volumes using a permutation method to obtain voxel-level corrected significance values (Holmes et al. 1996, Nichols and Holmes 2001)

robust relative to distributional assumptions and with good power (Nichols and Hayasaka 2003).

Results

Figure 1 gives an idea of what these images look like, when taken from a 3T scanner (details on the acquisition methods are in the Material and methods section). On the left, an arbitrarily chosen single acquisition is displayed. Each of these images is reconstructed from two original echo-planar imaging (EPI) scans, one of which taken after a labeling pulse, which tags the blood in the neck before it is distributed to the brain. The reconstruction of regional perfusion is accomplished on the basis of a compartment model (Wang et al. 2003). The image of a single acquisition demonstrates the large amount of noise in these data, at least as obtained in our laboratory. The low signal-to-noise ratio justifies relatively large voxel sizes in the acquisition. In the centre of Figure 1, an average image computed from 8 min. of acquisitions from the same subject. Given the constraints imposed by the labeling techniques (two EPI scans at TR = 4 sec each), 60 rCBF images were acquired in this time interval. On the right, the average rCBF obtained from the images acquired in this way from all 228 healthy adults in the sample of this study.

FIGURE 1 ABOUT HERE

Figure 1 shows the rCBF signal to be characterized by considerable instability at the edges and outside the brain. In the average perfusion images of a single individual (center), this instability is evident as a gross granularity of the signal at the brain edges. Figure 2 shows the standard deviation of these average perfusion images at three transversal slices, confirming the existence of high variance at the edges of the brain. This high variance at the edges is about one order of magnitude larger than within the brain, with the exception of some small brain structures (marked with red arrows in Figure 2), which are also characterized by high variance. Furthermore, within the brain the variance of the perfusion signal is smaller in white than in gray matter.

A possible concern regarding the high variance at the edges is that it may contaminate the cortical signal at the surface of the brain after smoothing. In the rest of this study, we masked the image at the edge using a threshold of a standard deviation of 25 ml dl^{-1} min^{-1}, since our interest focuses on the variance of the signal arising from within the brain.

The simple baseline study model

As noted in the Introduction, the variance of Figure 2 may be decomposed into two sources: acquisition-to-acquisition and subject-to-subject variance. The former is the variance arising from differences between each acquisition due to unaccounted effects and experimental error, while the latter is constituted by variation in brain perfusion among individuals. Formally, in a sample of $i = 1, 2, \ldots a$ subjects, in each of which $j = 1, 2, \ldots n$ acquisitions were made (each obtained from two scans, with and without labeling pulse), the data may be modeled voxel by voxel as follows:

$$y_{ij} = A_i + \varepsilon_{ij} , \qquad (1)$$

where y_{ij} is the preprocessed voxel signal, A_i is the perfusion signal in subject i, and ε_{ij} is an experimental error term introduced in each acquisition. The signal in each subject A_i is modelled as a random variable with mean μ (the overall mean signal level) and variance σ_A^2 (the subject-to-subject variation), assumed to be independent of the variance of the experimental errors σ^2 (the acquisition-to-acquisition variation). Because of the simple balanced structure of this model, σ_A^2 and σ^2 may be estimated from ordinary ANOVA mean sums of squares (Figure 3). If these sources of variance are normally distributed, these ANOVA estimates are also the restricted maximum likelihood estimates.

As it is immediately clear from Figure 3, subject-to-subject and acquisition-to-acquisition sources of variation are characterized by completely different spatial patterns. The

major pattern emerging from the subject-to-subject variance estimate of Figure 3 is increased variation in gray relative to white matter areas. Subject-to-subject variation is, therefore, an important source of the differences in variance between white and grey matter that were visible in Figure 2. Another noticeable feature of subject-to-subject variance is that rCBF appears to vary the most across individuals in the posterior part of the brain (cerebellum and posterior cortical areas, red arrows).

In contrast, the acquisition-to-acquisition variance is characterized, on the one hand, by variation at the edges of the brain that was not removed by the mask, and on the other hand, by areas of high variation on the midline, in the insular region, and in the lower portion of the brain. These latter areas correspond to the small structures inside the brain that displayed larger variance in Figure 2.

To better understand the origin of acquisition-to-acquisition variance, we acquired a smaller additional dataset of time-of-flight (TOF) angiography images (Figure 4). In these images, vessels are easily recognizable as brighter signal. One can see that the acquisition-to-acquisition high variance of the small structures within the brain has its source in large vessels. At the base of the brain, one can recognize the middle cerebral artery stemming from the internal carotid, the posterior cerebral artery, and the posterior sagittal sinus. Close to the midline, after normalization the middle cerebral artery runs in about the same position in all subjects, but more laterally the arteries diverge forming a dispersion fan before bending backwards, reflecting individual variation in their precise course. All these structures are matched by areas of comparatively larger acquisition-to-acquisition variance. Also at higher slices (Figure 4, centre and right), one can see that the increased acquisition-to-acquisition variance at the midline and in the insular region corresponds to important vascular structures, such as the insular arteries, and arteries on the midline (frontal and anterior cerebral arteries anteriorly, the pericallosal artery, and the middle occipital and choroidal arteries posteriorly).

Also venous sinuses, such as the posterior sagittal and the rectal sinus, lead to higher acquisition-to acquisition variance.

Some of the acquisition-to-acquisition variance visible in the bottom row of Figure 3, however, does not correspond to large vascular structures. This is the case for high variance regions at the edges of the brain, at the outer edge of the cerebellum and in the olfactory cortex, and in the posterior portion of the midline at $z = 24$ mm.

Impact of different sources of variation on second-level analyses

The 'first' and 'second level' approach to the estimation of the random effects model translates into averaging acquisitions in each individual for the first level step, before entering second level analysis. Let $\bar{A}_{i.}$ denote this averaged subject signal. Using standard ANOVA theory (see for example Frackowiak et al. 2003), it may be shown that

$$E\left(\mathrm{Var}(\bar{A}_{i.})\right) = \sigma_A^2 + \frac{1}{n}\sigma^2 . \tag{2}$$

This equation shows that the variance of the averaged subject images $\bar{A}_{i.}$ stems from both the acquisition-to-acquisition and the subject-to-subject sources of variance, even if the acquisition-to-acquisition variance is damped by the number of acquisitions.

The relation between the two variance components σ_A^2 and σ^2 of equation (2) is of help in estimating the relative effect of increasing the length of baseline acquisitions relative to increasing the number of subjects scanned in a simple baseline study (Snedecor and Cochran 1967). By increasing the number of acquisitions n, the contribution of the acquisition-to-acquisition variance to the variance of the average subject images $\bar{A}_{i.}$ decreases by a factor $1/n$. This is highly desirable, since the variance of the $\bar{A}_{i.}$'s accruing from σ^2 is assumed to be due to experimental error and will not be explained by between-subjects variables in the model. In the box plots on the left part of Figure 3, one can see that acquisition-to-acquisition

variance in most of the brain is one order of magnitude larger than subject-to-subject variance. In our data, n is 60, so that we may expect acquisition-to-acquisition variance in the average subject images $\overline{A}_{i.}$ to range from about $\sigma^2 = 20$ to $\sigma^2 = 38$ (1200 to 2300 divided by 60) in most of the brain, compared to the 80-160 range of subject-to-subject variation (the underlying rCBF estimates are expressed in ml dl^{-1} min^{-1}). Near large vessels the acquisition-to-acquisition variance is even higher, ranging from $\sigma^2 = 35$ to $\sigma^2 = 65$. The relatively large variance contributed by acquisitions-to-acquisition variance means that it may pay off to increase the duration of the baseline experiment for longer than the 8 min. used here (assuming that the underlying state remains stable for these longer periods of time). An optimal tradeoff in the sample size cannot be set *a priori* since it requires assigning a cost to increasing the number of acquisitions and a cost to recruiting more subjects.

The random effects model can also be used to obtain the precision of perfusion estimates. The expected variance of the estimated perfusion level in one voxel $\overline{y}_{..} = \sum_{i=1}^{a} \overline{A}_{i.}$ is given by

$$E\left(\text{Var}\left(\overline{y}_{..}\right)\right) = \frac{\sigma_A^2}{a} + \frac{\sigma^2}{an}. \tag{3}$$

To obtain an approximate confidence interval for an estimate of a change of perfusion levels $\beta = \overline{y}_{..} - \mu$, the standardized perfusion levels estimates are modeled with the Student's t distribution or, if the sample from which the estimates are taken is large enough, as a standard deviate z. Elementary sampling theory then provides the approximate number of subjects a or the number of scans n per subject required to estimate a change in perfusion with the desired precision (Snedecor 1946, pp. 456-458). Assuming our large-sample estimates $\hat{\sigma}_a^2$ and $\hat{\sigma}^2$ are good enough to approximate the variances that would be obtained, on average, in a new sample, the minimum required number of subjects a, given the number of acquisitions n, is given by:

$$a = \frac{z^2 \left(\hat{\sigma}_a^2 + n^{-1} \hat{\sigma}^2 \right)}{\beta^2} , \qquad (4)$$

and the minimum n given a by:

$$n = \frac{z^2 \hat{\sigma}^2}{\beta^2 a - z^2 \hat{\sigma}_a^2} . \qquad (5)$$

If the desired precision is expressed as percentage change in perfusion levels δ, the preceding equations are modified by replacing β with $\delta \overline{y}_{..}/100$.

Note that while it is always possible to improve the precision to any desired level by increasing the number of subjects in the sample, this will not in general be true for an increase of the number of acquisitions. Looking at equation (3), one can see that by changing the size of n one cannot compress the expected variance of $\overline{y}_{..}$ below σ_A^2/a.

In the top row Figure 5, we show maps of the number of subjects required to detect a $\delta = 10\%$ change in perfusion levels at the 5% confidence level (one-sided) in a sample of 60 acquisitions per subject, corresponding to sessions lasting 8 min. Because precision is expressed as percentage change, the requirements on the sample are more exacting for the white matter compartment, where absolute perfusion levels are lower and the change to detect is smaller in absolute terms. Here, samples of 60 subjects or more are required. In the gray matter compartment, in contrast, 10% precision is reached in samples of 30 to 40 subjects.

FIGURE 5 ABOUT HERE

In the bottom row of the same figure, we show the number of acquisitions required to achieve the same precision in a sample of 40 subjects. One can see that there are patches of the image in the white matter compartment where a sample of 40 cannot achieve 10% precision, irrespective of the number of acquisitions (in white), due to large subject-by-subject variance σ_A^2/a relative to the required precision. Around these patches, the required number of acquisitions increases without bounds since the desired precision is almost entirely offset

by the subject-by-subject variance σ_A^2/a. In contrast, in gray matter 30 to 40 acquisitions suffice to reach this precision level, with the exception of the areas in the temporal lobe located in proximity of large vessels.

Even if they both improve the precision of the estimate, it is important to note that increases of the sample size in acquisitions and in subjects are not entirely exchangeable. These increases involve changes in the representativeness of the sample for two dimensions of the underlying population that are entirely distinct. When baseline studies are used to investigate associations of perfusion levels with between-subjects variables, the systematic effects of the between-subjects variables explain part of the subject-to-subject variance, not part of the acquisition-to-acquisition (residual) variance (see Gelman and Hill 2007, pp. 263-264; Raudenbush and Bryk 2006, pp. 20-21). Acquisition-to-acquisition variance, however, causes uncertainties in the estimates of the average subject images $\overline{A}_{i.}$'s accounted for by the term σ^2/n in equation (2). Hence, increasing the number of acquisitions improves the fit by increasing the precision of the estimate of the average subject images $\overline{A}_{i.}$'s, while increasing the number of subjects improves power by increasing the degrees of freedom of the second-level fit of the $\overline{A}_{i.}$'s on the between-subjects variable. The implication of the model is that σ_A^2 contains variance that one is trying to explain, while σ^2 contains measurement error only, or the sum of innumerable effects that can be treated as random. For this reason, in the following we focus on the structure of subject-to-subject variance.

Spatial covariation of averaged subject images
The subject-to-subject variance component estimates displayed in Figure 3 provide no information on the way in which perfusion levels co-vary spatially across the brain. For example, even if it is clear that high variation characterizes most of the cortex, perfusion could be high in one cortical area and low in another in one subject, while in another subject the relation may be reversed. The net effect is that variation is high in both areas. The

alternative possibility is that some subjects have high signal, while other subjects low signal in all areas at the same time. This also results in high variation in the same cortical areas, but in each subject the signal is uniform, because it co-varies across voxels.

To distinguish between these possibilities and characterize the spatial co-variance of the signal, we carried out a principal component analysis of the averaged subject images (Figures 6 and 7). The scree plot of the eigenvalues, displayed in Figure 6, suggests that at least two components, explaining about 45% and 10% of the spatial variance, should be considered. The 'eigenimage' of the first component is of the same sign in the whole brain, capturing individual changes in the overall level of perfusion (Figure 7, top row). This component correlates very strongly gCBF ($r = 0.999$, $p < 0.001$). Furthermore, one can see that overall perfusion levels affect grey matter more than white matter, which is darker in the spatial map of Figure 7. This finding suggests that individual increases in gCBF translate in relatively higher perfusion values in the cortex and the basal ganglia, while the perfusion in the white matter is increased to a lesser degree.

FIGURE 6 ABOUT HERE

The 'eigenimage' of the second component (Figure 7, second row from top) demonstrates that the high intersubject variation in the posterior areas of the brain (previously detected in Figure 3, top row) is due to these regions being decoupled by the rest in terms of perfusion levels. The areas affected by this decoupling are those that are perfused by the posterior cerebral artery and its collaterals: the cerebellum, large part of the thalamus and some of the posterior striatum, the calcarine cortex and the medial part of the occipital cortex, the posterior cingulate and the adjacent medial portions of the parietal cortex.

FIGURE 7 ABOUT HERE

Even if they explain a relatively small portion of the overall variance in the principal component analysis, also the third and fourth components display a recognizable spatial pattern (Figure 7, lower half). The third component captures the lateralization of perfusion.

The fourth component contains variation with mostly the same spatial distribution as that arising from the course of large vessels. Like the third component, the fourth component shows also some lateralization. Especially the variance arising from the insular arteries, while present on both sides, is anticorrelated. The variance caused by large vessels may originate in acquisition-to-acquisition variance but, as we have seen in equation 2, the variance of the averaged baseline images is contaminated by this source of variance.

FIGURE 8 ABOUT HERE

Figure 8 displays the histograms of the first four component scores, which are the coefficients of the projection of the volumes on the direction in space of each component. The larger this coefficient, the more marked is the presence of the pattern of spatial distribution identified by each eigenimage. One can check that there are no extreme values that may determine alone the direction of any component.

Spatial components and individual variables

In studies of individual differences, between-subjects variables are correlated voxel by voxel with the observed average subject signal $\overline{A}_{i\cdot}$, explaining some of the subject-to-subject variance σ_A^2 contained in the variance of $\overline{A}_{i\cdot}$. Given that the principal component analysis revealed the existence of a spatial structure of σ_A^2, a question that arises naturally is the extent to which these patterns of variation correspond to variation associated with individual between-subject variables. To this end, we estimated the correlation between each component score and gCBF, age, and gender (see Methods for details), using a permutation technique to compute significance levels corrected for the multiple tests arising from the number of components tested (Table 1).

The first component (Figure 9) shows an extremely strong correlation with gCBF, as already mentioned; gCBF correlates with no other component. The first component also negatively correlates with age ($r = -0.17$, $p = 0.03$). Given the strong correlation between this first component and gCBF, this finding shows that older adults are characterized by decreased cerebral blood flow values as a whole.

The second component, which may reflect the vascular decoupling of the posterior cerebral artery from the rest of the brain, also correlates with age ($r = 0.18$, $p = 0.02$). The third component correlates with gender ($r = 0.29$, $p < 0.001$), suggesting an association between lateralization of perfusion and gender. Note that, with the exception of gCBF, all these correlations explain too small a portion of the variance identified by these components to conclude that they can be identified with the components themselves.

The fourth component shows little correlation with individual covariates. This may be due to this component containing prevalently acquisition-to-acquisition variation, which arises within subjects, while individual covariates are between-subjects variables. However, there is a trend for a weak association with gender ($r = 0.16$, $p = 0.05$), suggesting higher variation in males.

Impact of adjustment for global perfusion levels

Because of the high association between the scores on the first component and gCBF levels, when the principal component analysis was carried out after adjusting for gCBF, components were obtained that were virtually identical to those of the unadjusted data, with the exception of the first component, which had simply disappeared.

In our data one also finds that the statistical analysis is qualitatively changed by the adjustment for gCBF. This is the case because age competes with gCBF for explaining the variance captured by the first component (the amount of variance explained by these

individual variables may be obtained from Table 1 by squaring the correlation coefficients, since the correlations were computed separately). On its own, gCBF explains about 99% of this variance, while age independently explains 4% of it. Hence, some of the variance explained by gCBF must be shared with age. This is possible because age is itself correlated with gCBF ($r = -0.17$, $z = -2.50$, $p = 0.006$). Thus, the adjustment removes the variance in the data explained by age that loads on the first component, while leaving intact the variance in the second component.

We illustrate here this effect in Figure 10, which shows the parametric maps of the correlation between average subject rCBF and age, with and without adjustment for gCBF, thresholded at a liberal level to allow appreciation of the differences in the estimated maps. The map for the analysis without gCBF adjustment reveals that age affects perfusion negatively across the cortex, but much more markedly in the prefrontal regions, reaching voxel-level corrected significance in the anterior medial prefrontal cortex (supplementary motor area, BA32, x, y, $z = 2$, 12, 48, $t = -5.6$, $p < 0.001$, and pregenual cingulus, BA10-32, x, y, $z = 2$, 12, 48, $t = -5.8$, $p < 0.001$), in the lateral prefrontal cortex (BA44, x, y, $z = 52$, 20, 38, $t = -6.3$, $p < 0.001$), but also in posterior regions such as BA40 in the parietal cortex (x, y, $z = 58$, -38, 48, $t = -4.9$, $p = 0.006$). There is little evidence of increases in perfusion in the brainstem and the thalamic region (x, y, $z = 6$, -16, -12, $t = 2.8$, $p = 0.72$). Here and in the territory of the posterior cerebral artery perfusion is increased, but not significantly. In contrast, the gCBF-corrected analysis reveals a relative hyperperfusion in this whole territory, especially marked in thalamic, subthalamic and mesencephalic regions (x, y, $z = 6$, -16, -12, $t = 5.4$, $p = 0.01$; x, y, $z = 14$, -8, 2, $t = 5.1$, $p = 0.02$). There is still evidence of localized hypoperfusion in the prefrontal regions, which reaches voxel-level corrected significance in the medial prefrontal cortex (BA44, x, y, $z = 52$, 20, 38, $t = -6.5$, $p < 0.001$), but no evidence of reduced perfusion in more posterior regions (all significance levels reported here are voxel-level corrected; see the online supplementary data for the tabulation of the statistical analysis).

The persistence of a significant correlation between age and perfusion in the prefrontal region after adjustment suggests that the effect of age is not identical with the generic differences in cortical perfusion levels identified in the principal component analysis, but rather that it disproportionately affects the prefrontal cortex.

FIGURE 10 ABOUT HERE

Discussion

The baseline study design investigated here is formally characterized by the absence of within-subjects experimental variables. The primary data brought to second-level analysis for statistical inference are not estimates of contrasts between experimental conditions at the first level (as is commonly the case in functional imaging studies), but average subject perfusion levels to be correlated with individual between-subjects variables of interest. This design typically applies to studies of brain perfusion at rest. However, especially in the PET literature, studies can also be found in which subjects were asked to perform one simple task during all acquisitions. Because they lack within-subjects variables, the design of these studies is formally the same as the one examined here, even if the substantive interpretation of the results might differ.

This design typology contains two components of variance: subject-to-subject and acquisition-to-acquisition (residual). Attempts to reduce undesired variance can therefore be directed at either of these sources. In addition, experimenters may attempt to control variance by adjusting for global perfusion levels. It was shown that each of these sources of variance affect the data in different ways, and that the strategies to contain them are characterized by distinctive advantages and shortcomings.

In our data, the acquisition-to-acquisition variance was particularly strong at the edges of the brain, where the compartment model used to estimate perfusion may not deliver meaningful results, but also in correspondence of anatomical structures such as large vessels and venous sinuses. Since acquisition-to-acquisition variance negatively affects statistical

tests in the form of uncertainty in the estimate of the average perfusion levels brought to second level, the power of tests for differences in perfusion in these regions, i.e. in the anterior portion of the medial face of the temporal lobe, in the insula (especially posteriorly), and in parts of the cerebellum, may be reduced. Furthermore, we found an area of high variance in the hemispheric fissure arising from the numerous vessels in this region. This large variance levels might reduce power for the medial aspect of the cerebral cortex if large smoothing kernels are used.

The increased acquisition-to-acquisition variance near large vessels may be due to the 1 sec delay used in this study, which may be not long enough to allow all label to flow into capillary and tissue. Further studies should investigate the effect of increasing delay in reducing this aspect of acquisition-to-acquisition variance. Alternatively, acquisition-to-acquisition variance may be reduced by increasing the length of the measurement session, and this strategy appears to be especially meaningful if the regions where acquisition-to-acquisition variance is high are of specific interest. However, in this case one must assume that the mental state underlying perfusion levels is not changed by longer sessions.

An important shortcoming of the strategy of increasing the number of acquisitions is that it does not always replace the effect of increasing the number of subjects. Apart from the fact that one may be more interested in generalizing over subjects than over acquisitions, it was shown that the precision of the estimate cannot be compressed at arbitrarily low levels only by increasing session lengths. Our data showed that this may be a problem especially if one is interested in estimating perfusion at relative precision levels in the white matter.

In the second part of the study, we investigated the variance of the average perfusion volumes, which mainly contains subject-to-subject variance, and the effect of adjusting for global perfusion levels. The principal component analysis identified the major spatial patterns in which these images differ from each other. By far the largest source of variation in this respect was related to global perfusion levels, and revealed that these changes affect grey

more than white matter. Because scores on this first component were virtually identical to estimated gCBF levels, adjusting for gCBF led to the removal of this large component, indicating that the potential increases in power brought about by the adjustment are considerable.

Historically, the adjustment for gCBF through a covariate was justified by early reports showing that the global PET signal was essentially independent from regional PET signal changes arising from experimental manipulations (Friston et al. 1990, Ramsay et al. 1993). In the typical baseline study, there are no within-subjects experimental effects, while the variables of interest are between-subjects. Unfortunately, the case study of regression on age illustrates that there is no reason to assume these between-subjects variables to be uncorrelated with global perfusion levels, so that there may be genuine effects of interest in the correlation between gCBF and explanatory variables that are obliterated by the adjustment (see also Aguirre et al. 1998). Both analyses of the effect of age on rCBF, with and without adjustment, revealed different and potentially relevant aspects of the modulation of perfusion by age.

We also identified three further components of variation that affect baseline perfusion. One affected the brainstem, the thalami, and posterior parts of the brain comprising the calcarine and occipital cortex. These areas correspond to the territory of the posterior cerebral artery, suggesting a partial decoupling across subjects in levels of perfusion of these areas. This differential pattern of perfusion may be explained by the fact that the supply of the posterior cerebral artery differs markedly from the supply of the other arterial vessels of the brain. The posterior cerebral artery largely receives its supply by the vertebral arteries, and for a smaller, variable part from the internal carotid artery through the posterior communicans arteries. In contrast, the rest of the brain is supplied by the internal carotid only.

The effect of age in baseline metabolism or perfusion levels has been the subject of a considerable number of studies (see the reviews of Tumeh et al. 2007, Willis et al. 2002),

setting the stage for subsequent neuroimaging studies of the effect of age on performance (Rypma et al. 2006). Our data confirmed the findings reported in the literature. Our purpose was not to add to this considerable body of knowledge, but primarily that of illustrating the effects of adjusting for gCBF in the analysis. Findings based on the present sample, which is composed prevalently by young subjects, are not necessarily generalizable.

In the course of the analysis of the subject-to-subject variation, we also demonstrated an association between the degree of asymmetry of hemispheric perfusion and gender. This finding parallels similar finding on the effect of gender in asymmetry in structural images (Good et al. 2001, Toga and Thompson 2003, Narr et al. 2007) and in diffusion tractography (Catani et al. 2007). With respect of the design of baseline studies, these observations suggest that gender and age may be included as a nuisance covariate in the statistical analysis. The significance of these correlations, however, was predicated on the large size of the sample of this study. The amount of total variance explained by these individual variables remains small, suggesting that including them as nuisance covariates in the statistical analysis is not mandatory in general.

References

Abler, B., Hofer, C., Viviani, R., 2008. Habitual emotion regulation strategies and baseline brain perfusion. NeuroReport 19, 21-24.

Aguirre, G.K., Zarahn, E., D'Esposito, M., 1998. The inferential impact of global signal covariates in functional neuroimaging analysis. NeuroImage 8, 302-306.

Aguirre, G.K., Detre, J.A., Zarahn, E., Alsop, D.C., 2002. Experimental design and the relative sensitivity of BOLD and perfusion fMRI. NeuroImage 15, 488-500.

Arndt, S., Cizadlo, T., O'Leary, D., Gold, S., Andreasen, N.C., 1996. Normalizing counts and cerebral blood flow intensity in functional imaging studies of the human brain. NeuroImage 3, 175-184.

Beschoner, P., Richter, S., Lo, H., Sim, E.J., Baron, K., Osterfeld, N., Horn, A.B., Viviani, R., 2008. Baseline brain perfusion and working memory capacity: A neuroimaging study. NeuroReport (published online 30 October 2008).

Buxton, R.B., 2002. Introduction to Functional Magnetic Resonance Imaging. Principles and Techniques. Cambridge University Press, Cambridge.

Catani, M., Allin, M.P.G., Husain, M., Pugliese, L., Mesulam, M.M., Murray, R.M., Jones, D.K., 2007. Symmetries in human brain language pathways correlate with verbal recall. Proc. Natl. Acad. Sci. USA 104, 17163-17168.

Drevets, W.C., 2000. Neuroimaging studies of mood disorder. Biol. Psychiatry 48, 813-829.

Frackowiak, R.S.J., Friston, K.J., Frith, C., Dolan, R., Price, C.J., Zeki, S., Ashburner, J., Penny, W.D., 2003. Human Brain Function. Academic Press, London.

Friston, K.J., Firth, C.D., Liddle, P.F., Dolan, R.J., Lammertsma, A.A., Frackowiak, R.S.J., 1990. The relationship between global and local changes in PET scans. J. Cerebr. Bl. Flow Metab. 10, 458-466.

Gavrilescu, M., Shaw, M.E., Stuart, M.E., Stuart, G.W., Eckersley, P., Svalbe, I.D., Egan, G.F., 2002. Simulation of the effects of global normalization procedures in functional MRI. NeuroImage 17, 532-542.

Gelman, A., Hill, J., 2007. Data Analysis Using Regression and Multilevel/Hierarchical Models. Cambridge University Press, Cambridge (UK).

Good, C.D., Johnstrude, I., Ashburner, J., Henson, R.N.A., Friston, K.J., Frackowiak, R.S.J., 2001. Cerebral asymmetry and the effects of sex and handedness on brain structure. NeuroImage 14, 685-700.

Holmes, A.P., Blair, R.C., Watson, J.D.G., Ford, I., 1996. Nonparametric analysis of statistic images from functional mapping experiments. J. Cerebr. Bl. Flow Metab. 16, 7-22.

Jolliffe, I.T., 1986. Principal Component Analysis. Springer, Heidelberg.

Macey, P.M., Macey, K.E., Kumar, R., Harper, R.M., 2004. A method for removal of global effects from fMRI time series. NeuroImage 22, 360-366.

Mayberg, H.S., 2003. Positron emission tomography imaging in depression: A neural systems perspective. Neuroimaging Clin. N. Am. 13, 805-815.

Mumford, J.A., Hernandez-Garcia, L., Lee, G.R., Nichols, T.E., 2006. Estimation efficiency and statistical power in arterial spin labelling fMRI. NeuroImage 33, 103-114.

Narr, K.L., Bilder, R.M., Luders, E., Thompson, P.M., Woods, R.P., Robinson, D., Szeszko, P.R., Dimtcheva, T., Gurbani, M., Toga, A.W., 2007. Asymmetries of cortical shape: Effects of handedness, sex and schizophrenia. NeuroImage 34, 939-948.

Nichols, T.E., Hayasaka, S., 2003. Controlling the familywise error rate in functional neuroimaging: A comparative review. Statist. Meth. Med. Res. 12, 419-446.

Nichols, T.E., Holmes, A.P., 2001. Nonparametric permutation tests for functional neuroimaging: A primer with examples. Hum. Br. Mapping 15, 1-25.

O'Gorman, R.L., Kumari, V., Williams, S.C.R., Zelaya, F.O., Connor, S.E.J., Alsop, D.C., Gray, J.A., 2006. Personality factors correlate with regional cerebral perfusion. NeuroImage 31, 489-495.

Raichle, M.E., MacLeod, A.M., Snyder, A.Z., Powers, W.J., Gusnard, D.A., Shulman, G.L., 2001. A default mode of brain function. Proc. Natl. Acad. Sci. USA 98, 676-682.

Ramsay, S.C., Murphy, K., Shea, S.A., Friston, K.J., Lammertsma, A.A., Clark, J.C., Adams, L., Guz, A., Frackowiak, R.S.J., 1993. Changes in global cerebral blood flow in humans: Effect on regional cerebral blood flow during a nerual activation task. J. Physiol. (Lond) 471, 521-534.

Rao, H., Gillihan, S.J., Wang, J., Korczykowski, M., Sankoorikal, G.M.V., Kaercher, K.A., Brodkin, E.S., Detre, J.A., Farah, M.J., 2007. Genetic variation in serotonin transporter alters resting brain function in healthy individuals. Biol. Psychiatry 62, 600-606.

Raudenbush, S.W., Bryk, A.S., 2006. Hierarchical Linear Models: Applications and Data Analysis Methods. Sage Publ., (2nd ed.). Thousand Oaks.

Rypma, B., Berger, J.S., Prabhakaran, V., Bly, B.M., Kimberg, D.Y., Biswal, B.B., D'Esposito, M., 2006. Neural correlates of cognitive efficiency. NeuroImage 33, 969-979.

Shulman, G.L., Fiez, J.A., Corbetta, M., Buckner, R.L., Miezin, F.M., Raichle, M.E., Petersen, S.E., 1997. Common blood flow changes across visual tasks II. Decreases in cerebral cortex. J. Cognitive Neurosci. 9, 648-663.

Snedecor, G.W., 1946. Statistical Methods Applied by Experimenters in Agriculture and Biology (4th ed.). The Iowa State College Press, Ames (Iowa).

Snedecor, G.W., Cochran,, 1967. Statistical Methods. The Iowa State University Press, Ames (Iowa).

Toga, A.W., Thompson, P.M., 2003. Mapping brain asymmetry. Nature Reviews Neurosci. 4, 37-48.

Tumeh, P.C., Alavi, A., Houseni, M., Greenfield, A., Chryssikos, T., Newberg, A., Torigian, D.A., Moonis, G., 2007. Structural and functional imaging correlates for age-related changes in the brain. Semin. Nucl. Med. 37, 69-87.

Viviani, R., Grön, G., Spitzer, M., 2005. Functional principal component analysis of fMRI data. Hum. Br. Mapping 24, 109-129.

Wang, J., Alsop, D.C., Li, L., Listerud, J., Gonzalez-At, J.B., Detre, J.A., 2003. Arterial transit time imaging with flow encoding arterial spin tagging (FEAST). Magn. Reson. Med. 50, 599-607.

Wang, J., Zhang, Y., Wolf, R.L., Roc, A.C., Alsop, D.C., Detre, J.A., 2005. Amplitude-modulated continuous arterial spin-labeling 3.0-T perfusion MR imaging with a single coil: Feasibility study. Radiology 235, 218-228.

Willis, M.W., Ketter, T.A., Kimbrell, T.A., George, M.S., Herscovitch, P., Danielson, A.L., Benson, B.E., Post, R.M., 2002. Age, sex, and laterality effects on cerebral glucose metabolism in healthy adults. Psych. Res. Neuroimaging 114, 23-37.

Tables

Table 1. Correlation between component scores and individual covariates

	gCBF	Age	Gender
Component 1	$r = 0.99$, $z = 57.9$, $p < 0.001$	$r = -0.17$, $z = -2.62$, $p = 0.03$	$r = 0.13$, $z = 1.92$, $p = 0.20$
Component 2	$r = 0.02$, $z = 0.31$, $p = 0.99$	$r = 0.18$, $z = 2.78$, $p = 0.02$	$r = 0.01$, $z = 0.10$, $p = 0.99$
Component 3	$r = -0.01$, $z = -0.18$, $p = 0.99$	$r = 0.06$, $z = 0.89$, $p = 0.84$	$r = 0.29$, $z = 4.51$, $p < 0.001$
Component 4	$r \sim 0.00$, $z = 0.03$, $p \sim 1.00$	$r = 0.04$, $z = 0.54$, $p = 0.97$	$r = 0.16$, $z = 2.49$, $p = 0.05$

Explanation of symbols: z: Fisher's z-transformation of correlation coefficient; p: two-tailed significance level, corrected for the three repeated tests for each component.

Figure legends

Figure 1. From left to right: a single acquisition; the average perfusion in a single individual; and the overall average perfusion in the whole sample (Talairach coordinates: $z = 0$ mm). Data are in ml dl^{-1} min^{-1}. Negative CBF perfusion estimates tend to occur at the edges of the brain as a result of noise in the acquisition process exerting its effect through the perfusion estimates of the compartment model.

Figure 2. Standard deviation of average CBF images, computed from all 228 subjects in the sample. These images show that variance occurs at two orders of magnitude. Large variance (in yellow) is present at the edges of the brain and in correspondence of mall intracerebral structures, indicated with red arrows in the figure. Most of the brain parenchyma displays lower variance (in blue); within this area, one can easily distinguish white and grey matter.

Figure 3. On the left, box plots of voxel variance levels in subject-to-subject (top) and acquisition-to-acquisition volumes (bottom). Outliers (values beyond 1.5 times the interquartile range) are not shown to avoid clutter. Brain images show voxel by voxel estimates of σ_A^2, the subject-to-subject variance (top), and σ^2, the acquisition-to-acquisition variance (or modelled experimental error, bottom). Data were smoothed with a kernel of full-width-half-maximum (FWHM) of 6 mm.

Figure 4. Normalized TOF angiography images, showing areas where major vessels are located (brighter signal). The falciform structure within the brain parenchyma near the posterior edge of the brain (dark at $z = 0$ and 24) is a normalization artefact.

Figure 5. Maps of required sample sizes in subjects (top row) and acquisitions (bottom row) required to achieve a precision of 10% in perfusion estimates. See text for details.

Figure 6. Screeplot of the principal component analyses of the first ten components of the average baseline images.

Figure 7. Principal components of the mean baseline images. The images are scaled to the same vector length of 1, and the sign of the signal is arbitrary.

Figure 8. Histograms of the first four component scores. The projection of volumes on the eigenimages is unitless.

Figure 9. Plots illustrating the linear association between first component scores (in the ordinates) and gCBF (left), age (centre), and gender (right). The boxplot on the right is drawn at the lower and upper quartile values (boxes), with a line at the median value. The whiskers cover the extent of the rest of the data, with the exception of outliers (values beyond 1.5 times the interquartile range), which are marked with an 'x'.

Figure 10. Comparison of statistical parametric maps (thresholded at $p = 0.01$, uncorrected) for regression on age, adjusted for gender, without adjustment for gCBF (left), and with adjustment at second level (right). The lack of negative association between age and perfusion in the extreme frontopolar region, evident especially at $z = -11$ mm, is due to signal failure arising from a susceptibility artefact.

Figures
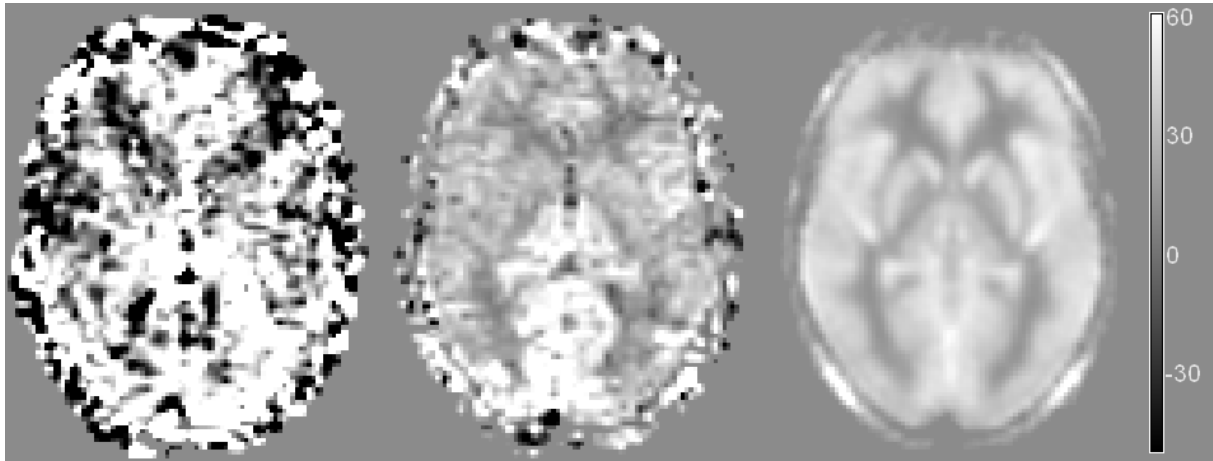
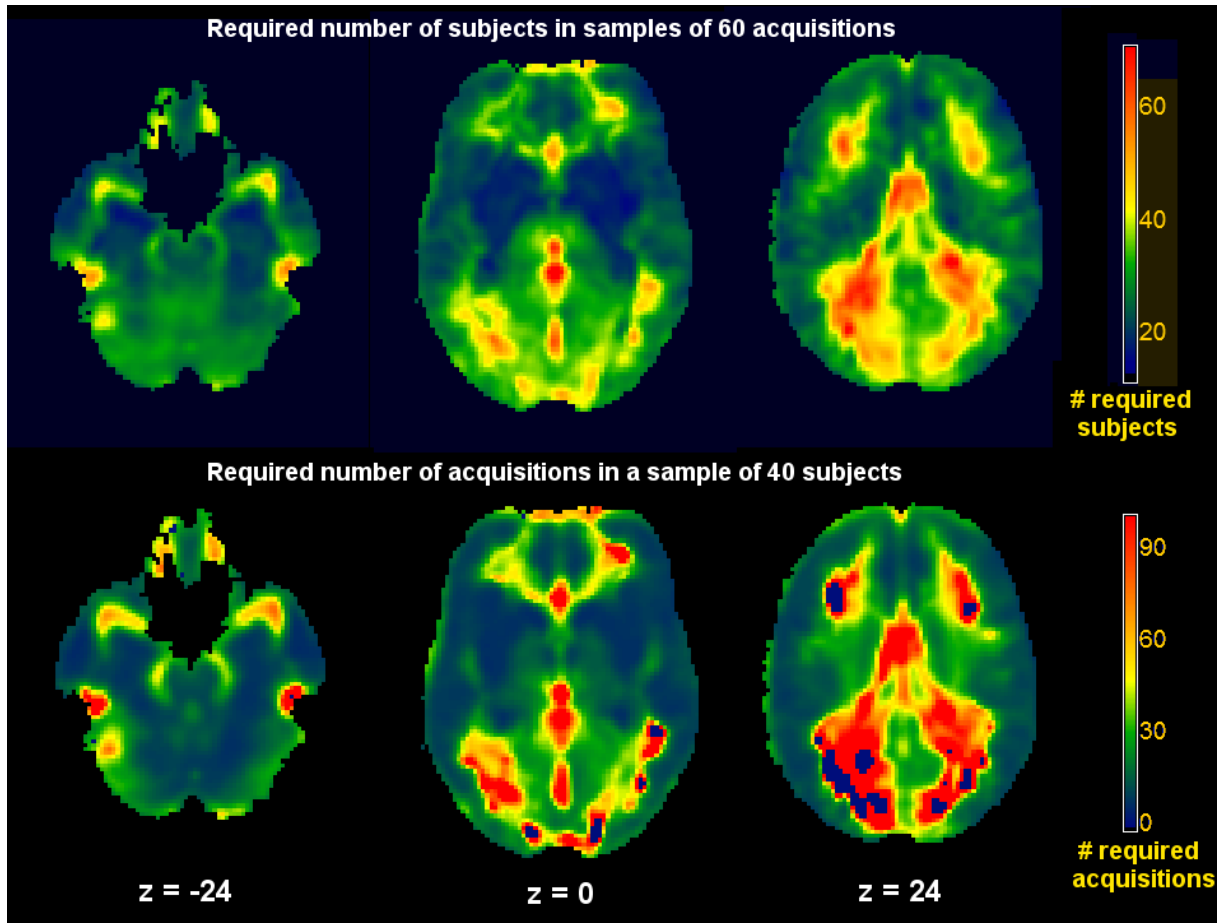
Figure 1
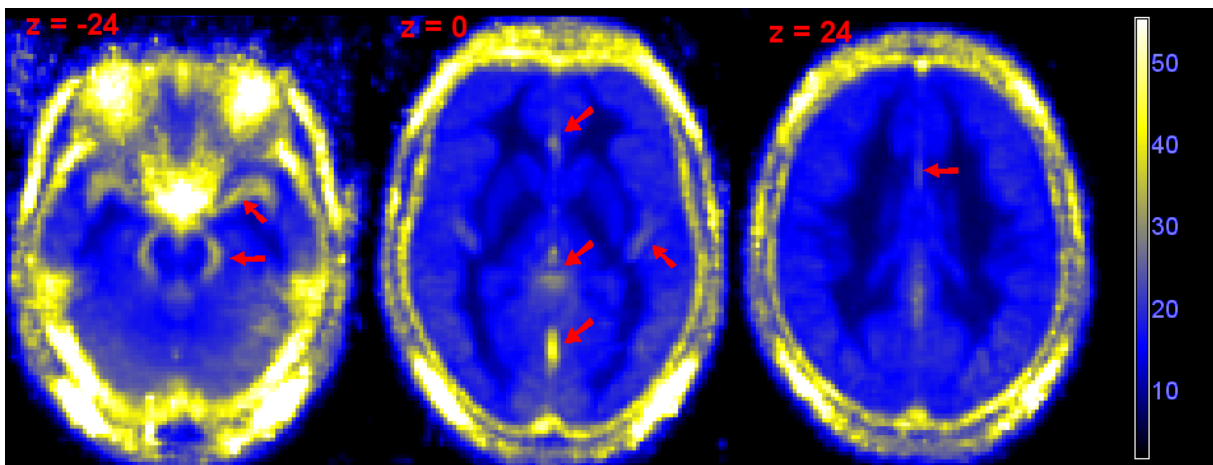
Figure 2

Figure 3

Figure 4

Required number of subjects in samples of 60 acquisitions

Required number of acquisitions in a sample of 40 subjects
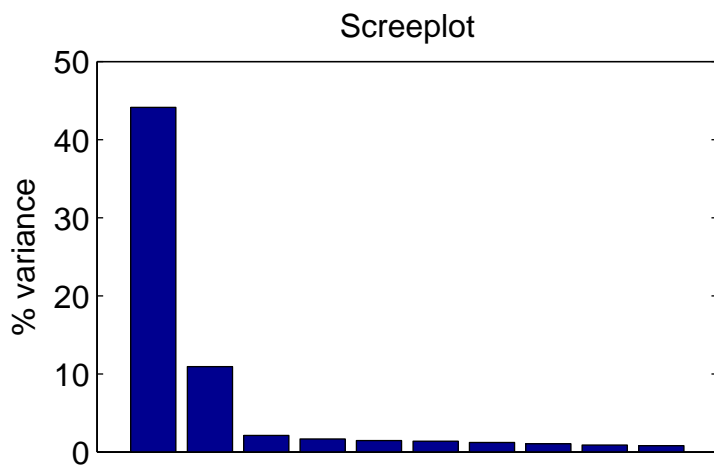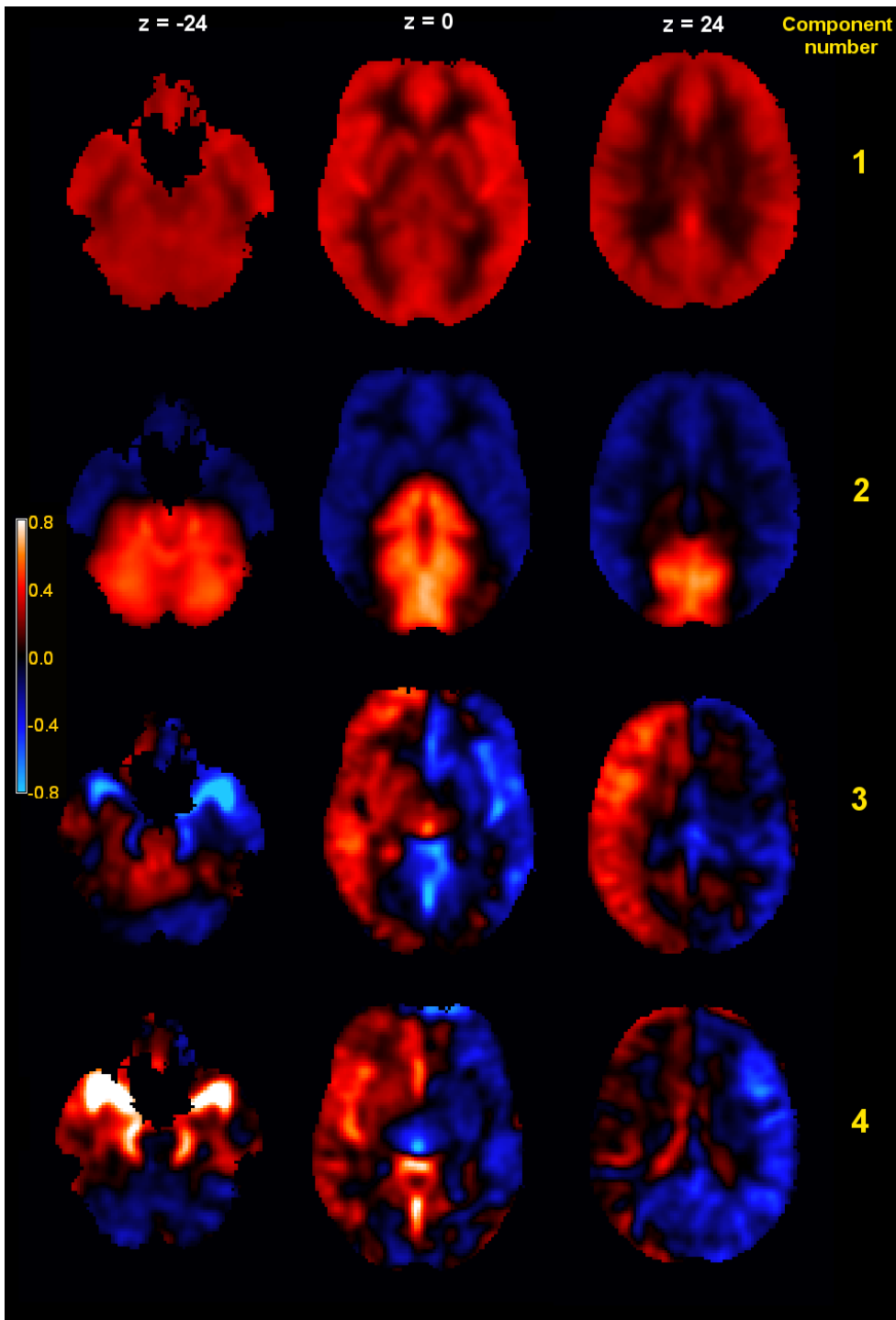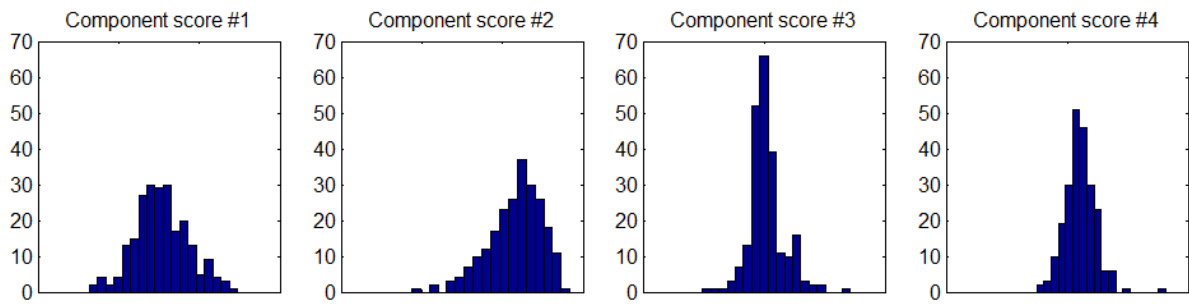
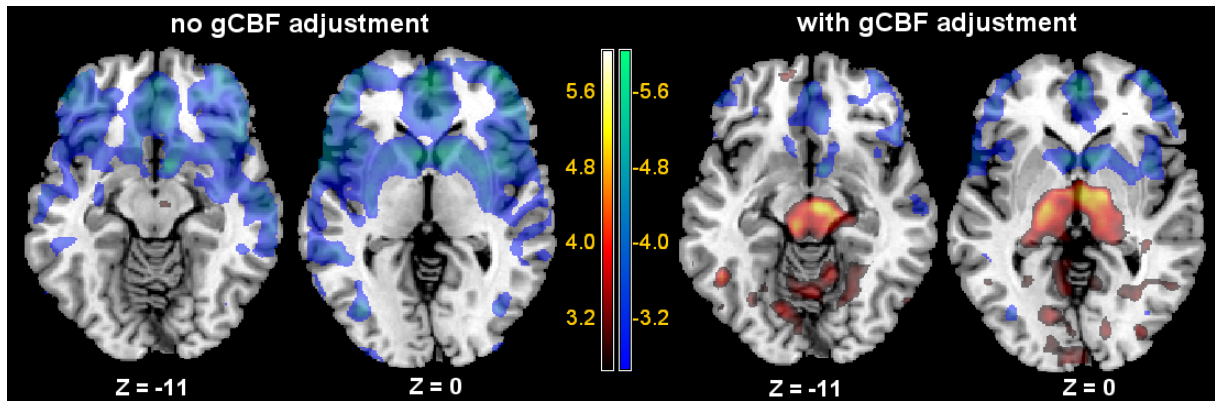z = -24   z = 0   z = 24

Figure 5

Screeplot
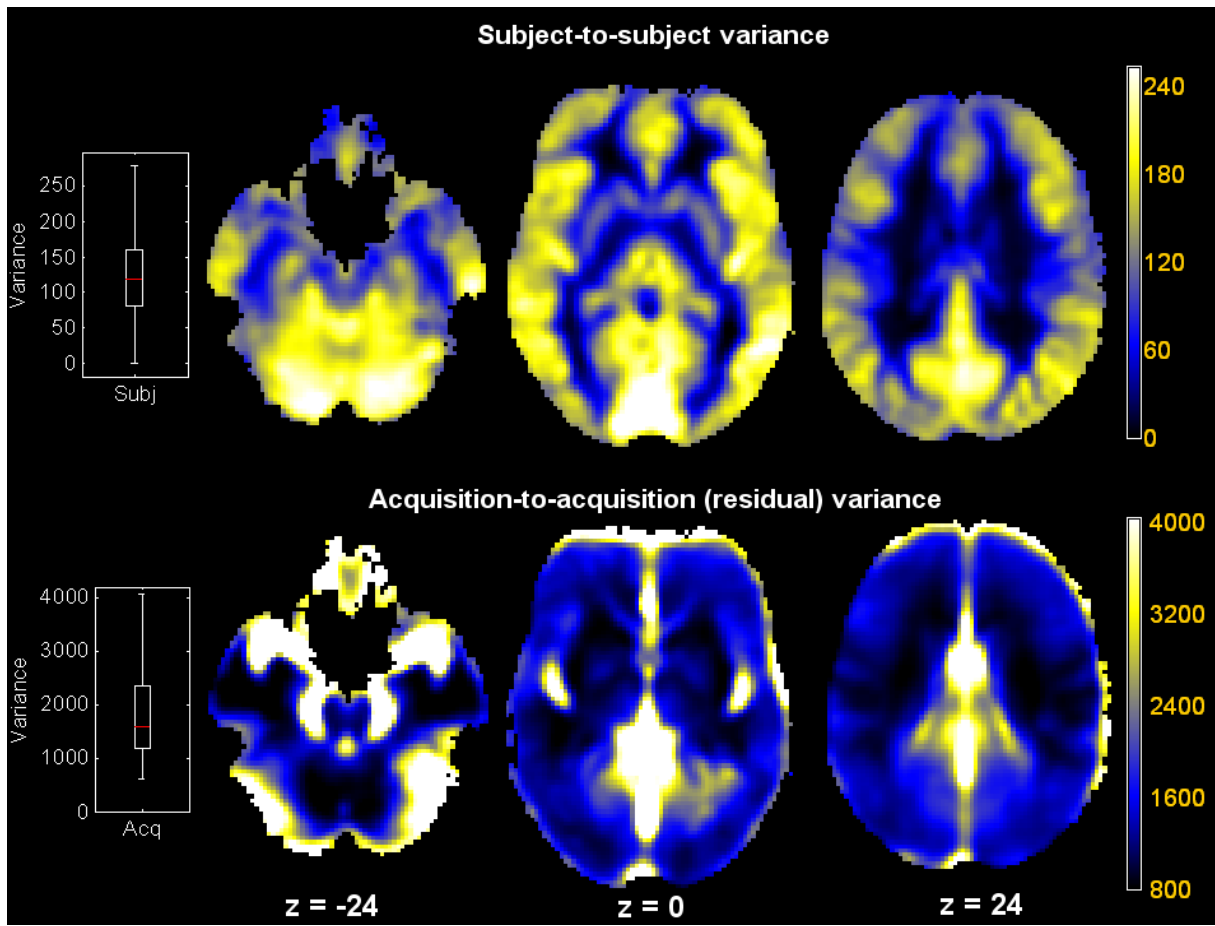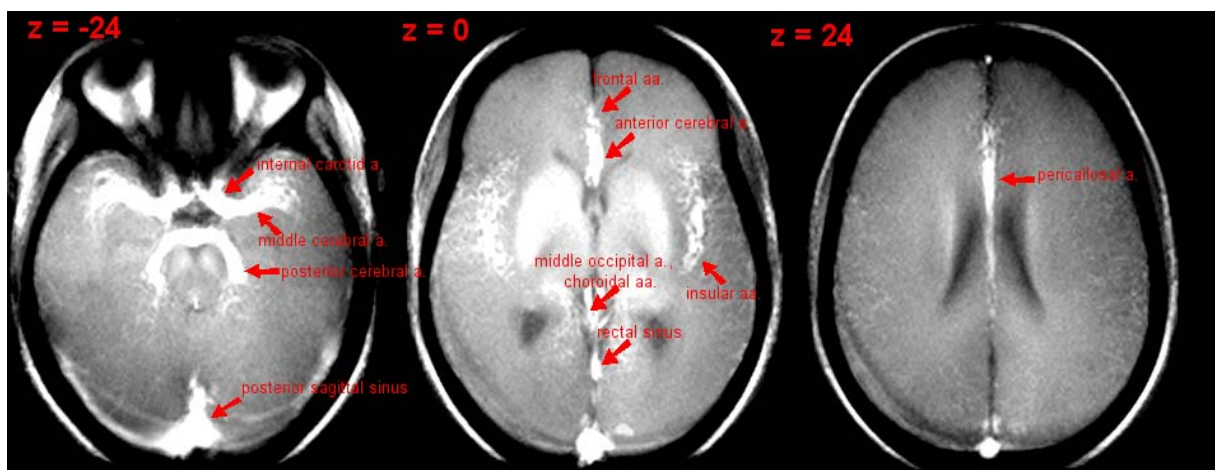
Figure 6

Figure 7

Figure 8

Figure 9

Figure 10